

## Thermochemistry and Electronic Structure of the Pyrrolyl Radical

Adam J. Gianola, Takatoshi Ichino, Rebecca L. Hoenigman, Shuji Kato, Veronica M. Bierbaum,\* and W. Carl Lineberger\*

JILA, University of Colorado and National Institute of Standards and Technology and Department of Chemistry and Biochemistry, University of Colorado, Boulder, Colorado 80309-0440

Received: May 21, 2004; In Final Form: August 25, 2004

The 364-nm photoelectron spectrum of pyrrolide anion, prepared by deprotonation of pyrrole, has been measured. The electron affinity (EA) of pyrrolyl radical has been determined to be  $2.145 \pm 0.010$  eV. Harmonic vibrational frequencies of  $925 \pm 65$ ,  $1012 \pm 25$ , and  $1464 \pm 20$   $\text{cm}^{-1}$  are observed in the spectrum of the  ${}^2A_2$  ground state of pyrrolyl. This spectrum is well reproduced by Franck–Condon fitting on the basis of the optimized geometries and the vibrational frequencies of the anion and the radical obtained at the B3LYP/6-311++G(d,p) level of density functional theory (DFT). The observed vibrational modes involve large displacements along the ring coordinates. While the Franck–Condon analysis also predicts a very similar spectrum for the  ${}^2B_1$  first excited state, only a broad, featureless, weak spectrum is observed near the calculated binding energy. The DFT calculations find a transition state for  ${}^2B_1$  electronic symmetry as a result of strong vibronic coupling between the  ${}^2A_2$  and  ${}^2B_1$  states. The transition state is located very close to a conical intersection of these states. The absence of distinctive features for the  ${}^2B_1$  transition state in the spectrum arises from the associated lifetime broadening. Using the EA of pyrrolyl together with the N–H bond dissociation energy (BDE) of pyrrole recently determined by Ashfold, the gas-phase acidity of pyrrole is  $\Delta_{\text{acid}}G_{298}(\text{RH}) = 351.9 \pm 0.4$   $\text{kcal mol}^{-1}$  and  $\Delta_{\text{acid}}H_{298}(\text{RH}) = 359.4 \pm 0.4$   $\text{kcal mol}^{-1}$ . The gas-phase acidity of pyrrole was also independently determined relative to methanethiol using a tandem flowing afterglow-selected ion flow tube. These measurements now provide a much more accurate set of benchmark acidities for pyrrole and methanethiol, a frequently employed reference acid.

### Introduction

Homonuclear polynitrogen compounds have been of interest to chemists for decades. Their decomposition reactions to form stable products, such as  $\text{N}_2$ , are highly exothermic, and hence these compounds are regarded as potential high-energy-density materials with nontoxic products. At the same time, the very high heat of formation and related instability have made experimental investigations of these compounds very difficult, and much of the work on this subject has been theoretical in nature.<sup>1–11</sup> Recently, however, there have been reports of the observation of relatively unstable polynitrogen species, including  $\text{N}_4$ ,<sup>12,13</sup>  $\text{N}_5^+$ ,<sup>14,15</sup>  $\text{N}_5^-$ ,<sup>16,17</sup> and  $\text{N}_6^-$ .<sup>18–20</sup> These reports encourage further investigation of the nature of these polynitrogen compounds.

One of these species,  $\text{N}_5^-$ , was detected through collision-induced dissociation electrospray ionization mass spectrometry<sup>16</sup> and laser desorption ionization time-of-flight mass spectrometry<sup>17</sup> of substituted *p*-phenylpentazoles. Theoretical studies suggest that  $\text{N}_5^-$  is stable as a cyclic form, pentazolide.<sup>7,10</sup> Its decomposition into azide anion and dinitrogen is predicted to be exothermic by  $14\text{--}16$   $\text{kcal mol}^{-1}$ , and the heat of formation of pentazolide is predicted to be  $\Delta H_f^\circ = 62.1 \pm 3.6$   $\text{kcal mol}^{-1}$ .<sup>7</sup> It is challenging to measure these thermodynamic values of pentazolide through experiments, considering the difficulty in its synthesis. Unequivocal synthesis or observation of pentazole,  $\text{N}_5\text{H}$ , has not yet been reported.<sup>21</sup>

One experimental approach is pursued here for the possible ultimate characterization of pentazolide and pentazole. Penta-

zolide and pentazole are nitrogen analogues of cyclopentadienide,  $\text{C}_5\text{H}_5^-$ , and cyclopentadiene,  $\text{C}_5\text{H}_6$ , respectively. Basic thermodynamic properties of  $\text{C}_5\text{H}_5^-$ , such as its proton affinity<sup>22</sup> and electron binding energy,<sup>23</sup> have been determined experimentally. In addition to these homonuclear species, heteronuclear five-membered ring compounds exist with different combinations of the number of C and N atoms. By investigating the thermodynamic properties of these heterocyclic compounds, we hope to learn about pentazolide and pentazole by extrapolation. In this spirit, we have initiated a systematic investigation of nitrogen-containing, five-membered heterocyclic compounds.

As a first step, we have investigated pyrrole,  $\text{C}_4\text{H}_5\text{N}$ . The gas-phase acidity of pyrrole relative to methanethiol ( $\text{CH}_3\text{SH}$ ) has been determined using a flowing afterglow-selected ion flow tube (FA-SIFT) instrument. Photoelectron spectra of the corresponding anion, pyrrolide, were measured to determine the electron affinity (EA) of pyrrolyl radical. The  $\Delta_{\text{acid}}G_{298}$  and EA are related to the bond dissociation energy (BDE, i.e., dissociation enthalpy at 0 K,  $DH_0(\text{R-H})$ ) for the N–H bond through a thermochemical cycle.<sup>24–26</sup> As Ashfold<sup>27</sup> has very recently determined the N–H bond strength of pyrrole with very high accuracy, we can now use this cycle to obtain improved values for the gas-phase acidity of the reference acids, pyrrole and methanethiol.

Measurements of photoelectron spectra are also valuable in that insight into the molecular structure can be obtained. Generally, Franck–Condon profiles in negative ion photoelectron spectra not only provide information about the vibrational frequencies of certain normal modes (usually totally symmetric modes) of the neutral radical but also indicate the magnitude

\* Authors to whom correspondence should be addressed. E-mail: wcl@jila.colorado.edu; Veronica.Bierbaum@Colorado.edu.

of the structural change between the anion and the neutral radical along those normal coordinates.<sup>28</sup> The photoelectron spectrum of pyrrolide shows remarkable differences between transitions to the ground state (<sup>2</sup>A<sub>2</sub>) and the first excited state (<sup>2</sup>B<sub>1</sub>) of pyrrolyl. The latter is very substantially broadened as a result of strong vibronic coupling, in a pseudo-Jahn–Teller interaction.

After describing the experimental techniques, we present the results of the photoelectron spectroscopy measurements followed by the gas-phase acidity measurements. The analysis of the experimental results is supported with *ab initio* and density functional theory (DFT) calculations. The effects of vibronic coupling on the adiabatic potential energy surface and the location of a conical intersection between the ground and first excited state of pyrrolyl are discussed in some detail.

## Experimental Methods

**Negative Ion Photoelectron Spectroscopy.** Ultraviolet negative ion photoelectron spectra of pyrrolide have been obtained with a photoelectron spectrometer that has been described in detail previously.<sup>28–30</sup> Briefly, pyrrole (Sigma, 98%) is introduced downstream of a microwave discharge flowing afterglow ion source where it undergoes a proton abstraction reaction with hydroxide in approximately 0.5 Torr of helium. Collisions with the helium buffer gas cool the ions to a vibrational temperature of ~298 K. The anions are extracted from the flowing afterglow region, accelerated to 736 eV, and focused for mass selection into a Wien velocity filter. The mass selected ions are then refocused, decelerated to 40 eV, and crossed with a photon beam from a cw argon ion laser (363.8 nm) in an external build-up cavity with a circulating power of approximately 100 W. A typical pyrrolide beam current is 150 pA. Photoelectrons collected in a direction perpendicular to the ion and laser beams are focused, passed through a hemispherical energy analyzer with 10–15 meV resolution, and imaged onto a position sensitive detector after amplification with microchannel plates. Spectra are obtained by measuring photoelectron counts as a function of electron kinetic energy (eKE). Subtraction of the electron kinetic energy from the photon energy converts the energy scale of the spectrum to electron binding energy (eBE).

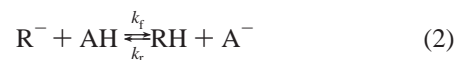
The energy scale is calibrated with the EA of atomic oxygen in the measurement of the photoelectron spectrum of oxygen anion.<sup>31</sup> A small (<1%) energy compression factor is applied as determined from the comparison of the photoelectron spectrum of tungsten anion with known energy levels of tungsten atom.<sup>32</sup> To obtain photoelectron angular distributions, a rotatable half-wave plate is inserted into the laser path before the build-up cavity. Spectra are obtained with laser polarizations parallel (0°), perpendicular (90°), and at the magic angle (54.7°) to the photoelectron collection axis. It has been shown<sup>33</sup> that the photoelectron angular distribution can be expressed as

$$I(\theta) = \frac{\sigma}{4\pi} [1 + \beta \cdot P_2(\cos\theta)] \quad (1)$$

where  $\theta$  is the angle between the laser electric field and the photoelectron collection axis,  $\sigma$  is the total photodetachment cross section,  $\beta$  is the anisotropy parameter, and  $P_2(\cos\theta)$  is the second-order Legendre polynomial. Measurements at these three polarization angles allow determination of the anisotropy parameter with some redundancy.

**Flowing Afterglow-Selected Ion Flow Tube Measurements.** The gas-phase acidity of pyrrole was measured using a tandem flowing afterglow-selected ion flow tube (FA-SIFT) instrument.<sup>34,35</sup> The forward ( $k_f$ ) and reverse ( $k_r$ ) rate constants were measured at 298 K for proton-transfer reactions between

pyrrole (RH) and a reference acid (AH). The ratio of the rate constants gives the proton-transfer equilibrium constant  $K_{\text{equil}}$  ( $\equiv k_f/k_r$ ).



The reactant anions (R<sup>−</sup> or A<sup>−</sup>) were generated in the source flow tube using hydroxide deprotonation of the corresponding neutrals, RH and AH. The ions were mass selected and injected into the second flow tube at low injection energies to minimize fragmentation. The reactant anions were thermally equilibrated with the helium buffer gas (0.5 Torr) before undergoing proton-transfer reactions with a neutral reagent, which was added through each of the multiple inlets located downstream along the flow tube. Depletion of the reactant ion signal was recorded with the detection quadrupole mass filter as a function of the inlet position (i.e., the reaction distance) and the reaction rates determined.<sup>34,35</sup> Measured rate constants are reproducible to within 3% (one standard deviation) and are reported with the statistical uncertainties in the present article. The rates also typically have absolute (systematic) error bars of ±20%. The systematic errors cancel in the rate constant ratio so that  $K_{\text{equil}}$  is determined very accurately. When the acidity of the reference acid,  $\Delta_{\text{acid}}G_{298}(\text{AH})$ , is known, the acidity of the RH molecule is determined from the equilibrium constant via the expression

$$\Delta_{\text{acid}}G_{298}(\text{RH}) = \Delta_{\text{acid}}G_{298}(\text{AH}) + RT \ln K_{\text{equil}} \quad (3)$$

The gas-phase acidity,  $\Delta_{\text{acid}}G_{298}(\text{RH})$ , is the free-energy change for the process  $\text{RH} \rightarrow \text{R}^- + \text{H}^+$ , where H is the most acidic hydrogen (N–H in this case). Methanethiol was used as a reference acid [ $\Delta_{\text{acid}}G_{298}(\text{CH}_3\text{SH}) = 350.6 \pm 2.0 \text{ kcal mol}^{-1}$ ].<sup>36</sup> The collision rate for pyrrole was calculated via the parametrized trajectory collision rate theory<sup>37</sup> using a polarizability<sup>38</sup> of  $8.03 \times 10^{-24} \text{ cm}^3$  and an electric dipole moment of 1.74 D.<sup>39</sup>

## Results

**Photoelectron Spectra.** The 363.8-nm (3.408 eV) magic-angle photoelectron spectrum of pyrrolide at ~298 K is shown in Figure 1a. The spectrum shows a Franck–Condon envelope with at least three active vibrations. The peak at  $2.145 \pm 0.010$  eV is assigned as the electronic band origin, corresponding to the EA of pyrrolyl. This value is close to that of  $2.39 \pm 0.13$  eV obtained by Brauman in a very early, low-resolution photodetachment measurement.<sup>40</sup> Three pyrrolyl vibrational frequencies are resolved in the spectrum,  $925 \pm 65 \text{ cm}^{-1}$ ,  $1012 \pm 25 \text{ cm}^{-1}$ , and  $1464 \pm 20 \text{ cm}^{-1}$ . Comparison between this spectrum and the spectrum measured at 200 K (not shown) identifies a weak peak at a lower binding energy as a pyrrolide vibrational hot-band with a frequency of  $874 \pm 95 \text{ cm}^{-1}$ . Measurements of the photoelectron angular distribution yield a value of approximately −0.5 for the anisotropy parameter,  $\beta$ , for the main features in the spectrum. The  $\beta$  value, however, gradually decreases across the weak continuous portion of the spectrum (eBE > 2.5 eV), approaching zero at 2.8 eV. This variation of  $\beta$  suggests that the spectrum may represent electron detachment from more than one molecular orbital of pyrrolide, as demonstrated below.

To aid in the assignment and interpretation of the photoelectron spectra, electronic structure calculations for pyrrolide and pyrrolyl were completed using the Gaussian 98 suite of programs.<sup>41</sup> DFT geometry optimizations were carried out with Becke's hybrid three-parameter functional<sup>42</sup> and the correlation functional of Lee et al.<sup>43</sup> (B3LYP). A vibrational analysis was

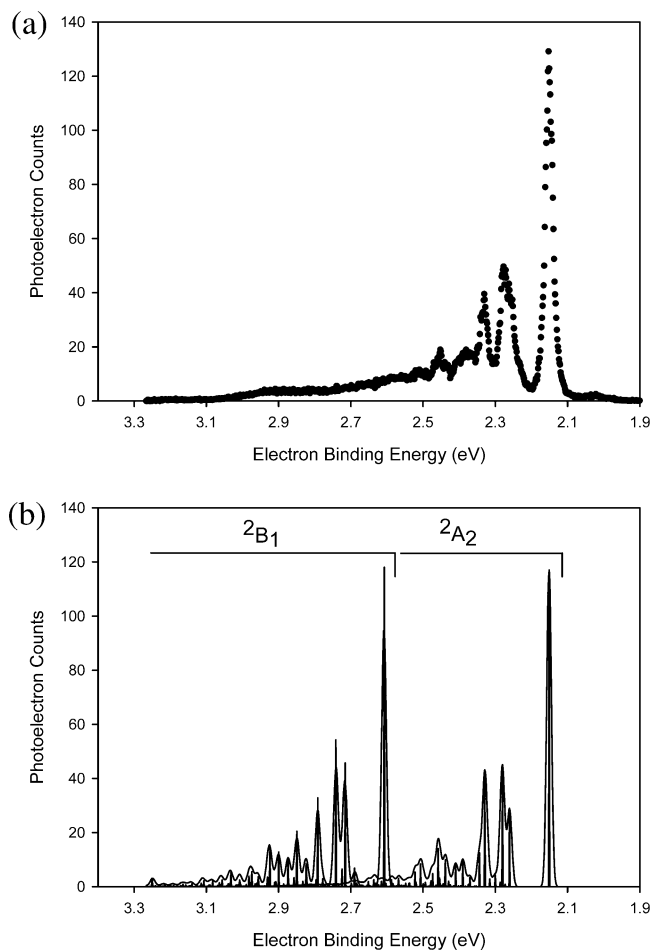


**Figure 1.** (a) 363.8-nm magic-angle photoelectron spectrum of pyrrolide anion. (b) Simulated photoelectron spectrum of pyrrolide using results from the DFT calculations. The sticks are the raw Franck–Condon factors and the solid curves are 15 meV fwhm Gaussian convolutions. In the simulated spectrum, the binding energy for the  ${}^2A_2$  origin peak was set to the origin peak observed experimentally. The binding energy for the  ${}^2B_1$  origin peak was set according to the term energy obtained in the DFT calculations (0.49 eV).

performed at each stationary point to confirm its identity as a minimum or a saddle point. The vibrational analysis also provides the zero-point and thermal energy corrections that are necessary to convert the B3LYP electronic energies to enthalpies at 298 K. The calculations reported here all employed the 6-311++G(d,p) basis set.<sup>44</sup>

The DFT calculations show that the ground state of pyrrolide has  $C_{2v}$  symmetry ( ${}^1A_1$  electronic symmetry). Figure 2 depicts the highest occupied molecular orbitals of the ground state of pyrrolide. The two highest occupied molecular orbitals ( $a_2$  and  $b_1$ ) are  $\pi$  orbitals, while the third highest occupied molecular orbital ( $a_1$ ) is a  $\sigma$  orbital. Clearly, detachment of an electron from the highest occupied molecular orbital forms the ground state of pyrrolyl with  $A_2$  electronic symmetry. Likewise, detachment from the second highest occupied molecular orbital forms the first excited state ( ${}^2B_1$ ). Detachment from the  $\sigma$  orbital is inaccessible with the photon energy of 3.408 eV used in the current experiment. The DFT calculations with  $C_{2v}$  geometries find a minimum with  ${}^2A_2$  electronic symmetry and a transition state with  ${}^2B_1$  electronic symmetry for pyrrolyl. These two stationary points are connected via a pseudorotation path on the ground adiabatic potential energy surface (vide infra). The DFT optimized geometries are given in Table 1. The optimized geometries for the ground states of pyrrolide and pyrrolyl are

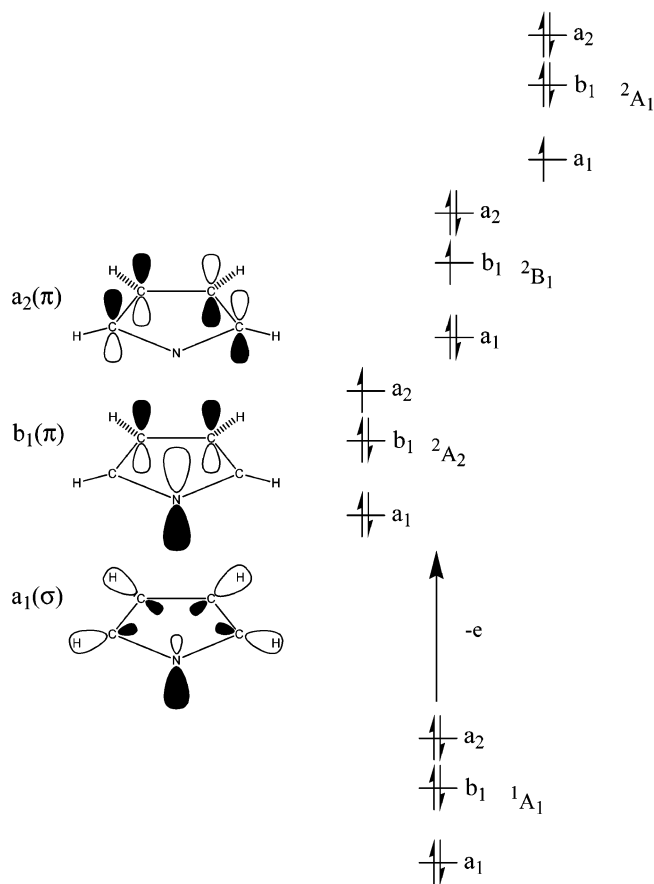


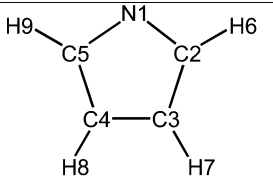
**Figure 2.** Three highest occupied molecular orbitals of pyrrolide, and the schematic representation of electron photodetachment from pyrrolide to form three electronic states of pyrrolyl.

in good agreement with B3LYP calculations by Schaefer.<sup>45</sup> Examination of the geometries provides insight into which vibrational modes will be activated upon photodetachment. There are significant differences of the bond lengths in the ring between the anion ground state and the two states of the radical. Therefore, it is expected that those vibrational modes which contain significant motion along the ring coordinates will manifest themselves in the Franck–Condon profile.

Using the geometry and frequency results from the DFT calculations, Franck–Condon factors were calculated for transitions from the  ${}^1A_1$  ground state of the anion to the  ${}^2A_2$  and  ${}^2B_1$  states of the radical with the PESCAL program,<sup>46,47</sup> assuming identical total photodetachment cross sections for the two radical states.<sup>48</sup> Figure 1b shows the raw Franck–Condon factors (sticks) and a 15 meV fwhm Gaussian line shape convolution (solid lines). Three totally symmetric vibrational modes in each state of pyrrolyl are determined to be active in the Franck–Condon profile; the corresponding normal mode displacements for the  ${}^2A_2$  state are depicted in Figure 3.

Comparison between the photoelectron spectrum (Figure 1a) and the Franck–Condon simulation (Figure 1b) makes it clear that the main features in the photoelectron spectrum can be ascribed to the  ${}^2A_2$  ground state of pyrrolyl. The DFT calculations predict an EA of 2.12 eV for pyrrolyl, in excellent agreement with the experimental value,  $2.145 \pm 0.010$  eV. The Franck–Condon analysis predicts the  ${}^2B_1$  state to appear in the spectrum as well (Figure 1b),<sup>48</sup> with a term energy for the  ${}^2B_1$  state calculated to be 0.49 eV at the B3LYP/6-311++G(d,p) level of theory.<sup>49</sup> However, no such prominent feature appears in the spectrum. The absence of distinctive features for the  ${}^2B_1$  state must originate from lifetime broadening along the normal

TABLE 1: Geometry Parameters for Pyrrolide and Pyrrolyl<sup>c</sup>

	pyrrolide	pyrrolyl		
	<sup>1</sup> A <sub>1</sub> <sup>a</sup>	<sup>2</sup> A <sub>2</sub> <sup>a</sup>	<sup>2</sup> B <sub>1</sub> (TS) <sup>a</sup>	Conical intersection <sup>b</sup>
N1—C2 and N1—C5	1.3625	1.3441	1.3856	1.3804
C2—C3 and C5—C4	1.4035	1.4598	1.3639	1.3759
C3—C4	1.4195	1.3610	1.4947	1.4779
C2—H6 and C5—H9	1.0865	1.0834	1.0794	1.0798
C3—H7 and C4—H8	1.0847	1.0798	1.0806	1.0804
∠C5-N1-C2	105.13	104.74	106.84	106.59
∠N1-C2-C3 and ∠N1-C5-C4	112.06	112.38	111.04	111.21
∠C2-C3-C4 and ∠C3-C4-C5	105.38	105.25	105.54	105.50
∠N1-C2-H6 and ∠N1-C5-H9	120.54	120.99	120.05	120.17
∠C2-C3-H7 and ∠C5-C4-H8	127.20	126.26	128.29	128.03

<sup>a</sup> C<sub>2v</sub> stationary points optimized with B3LYP/6-311++G(d,p). <sup>b</sup> See the text for derivation of the conical intersection geometry. <sup>c</sup> Bond lengths are in units of Å, and bond angles are in units of degree.

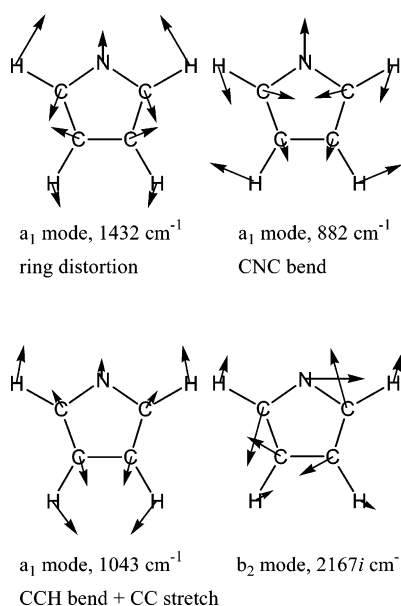


**Figure 3.** Relative atomic displacements in the normal modes for pyrrolyl radical. Three a<sub>1</sub> modes for the <sup>2</sup>A<sub>2</sub> state of pyrrolyl which are active in the photoelectron spectrum, and one b<sub>2</sub> mode for the <sup>2</sup>B<sub>1</sub> state of pyrrolyl which has an imaginary frequency. The harmonic frequencies are the DFT results (unscaled).

mode with an imaginary frequency. This point will be explained in the Discussion section.

**Gas-Phase Acidity.** The forward rate constant (eq 2) was measured for the reaction between pyrrolide and CH<sub>3</sub>SH, where the former was injected at  $E_{inj} = 20$  eV; negligible fragmentation was observed at this injection energy. For reactions of pyrrolide with CH<sub>3</sub>SH and pyrrole with CH<sub>3</sub>S<sup>-</sup>, the overall rate constants including proton transfer and adduct formation were measured to be  $7.56 \pm 0.21 \times 10^{-10}$  cm<sup>3</sup> s<sup>-1</sup> and  $4.91 \pm 0.10 \times 10^{-10}$  cm<sup>3</sup> s<sup>-1</sup>, respectively. The reaction of pyrrolide with CH<sub>3</sub>SH is faster than the reverse reaction, indicating that the forward direction is exoergic in the proton-transfer equilibrium. Using these rate constants, the gas-phase acidity,  $\Delta_{acid}G_{298}(\text{pyrrole})$ ,

is thus derived as  $350.9 \pm 2.0$  kcal mol<sup>-1</sup>. The dominant uncertainty in this value is the acidity of the reference acid, CH<sub>3</sub>SH. While true rate constants for proton-transfer reactions can be obtained from the overall rate constants by taking account of adduct formation, such a correction makes a negligible difference (<0.05 kcal mol<sup>-1</sup>) in  $\Delta_{acid}G_{298}(\text{pyrrole})$ . The experimental value of the gas-phase acidity of pyrrole given here is in excellent agreement with previous measurements,<sup>22</sup>  $353.0 \pm 2.0$  kcal mol<sup>-1</sup>. When shifted because of updates in the relative acidity scale, the previous measurement becomes identical to the current measurement,  $350.9 \pm 2.0$  kcal mol<sup>-1</sup>.<sup>36</sup>

The N—H bond enthalpy at the 0 K limit (i.e., the bond dissociation energy) has recently been measured accurately by Ashfold et al., using H atom-detected photofragment translational energy release spectroscopy.<sup>27</sup> This new value of  $4.073 \pm 0.005$  eV ( $93.92 \pm 0.11$  kcal mol<sup>-1</sup>) allows determination of the gas-phase acidity of pyrrole very accurately, using the following thermochemical cycle:

$$\Delta_{acid}H_0(\text{RH}) = IE(\text{H}) + D_0(\text{R-H}) - EA(\text{R}) \quad (4)$$

Here,  $\Delta_{acid}H_0(\text{RH})$  is the 0 K enthalpy of deprotonation,  $EA(\text{R})$  is the radical electron affinity,  $D_0(\text{R-H})$  is the bond dissociation energy, and  $IE(\text{H})$  is the ionization energy of the hydrogen atom (13.59844 eV). The 0 K enthalpy of deprotonation,  $358.0 \pm 0.4$  kcal mol<sup>-1</sup>, is related to the 298 K value through integrated heat capacities:

$$\Delta_{acid}H_{298}(\text{RH}) = \Delta_{acid}H_0(\text{RH}) + \int_0^{298} dT[C_p(\text{R}^-) + C_p(\text{H}^+) - C_p(\text{RH})] \quad (5)$$

The heat capacity integral was evaluated using the thermochemical information obtained as a part of the output of the Gaussian calculations described here. Conversion to the gas-phase acidity,  $\Delta_{acid}G_{298}(\text{RH})$ , is carried out using the entropy term  $T\Delta_{acid}S_{298}$ , which is also derived from the DFT calculations. In this way,  $\Delta_{acid}G_{298}(\text{RH})$  is determined to be  $351.9 \pm 0.4$  kcal mol<sup>-1</sup>. The gas-phase acidity determined independently from the equilibrium measurements,  $350.9 \pm 2.0$  kcal mol<sup>-1</sup>, is less



**TABLE 2: Thermochemical Parameters for Pyrrole and Pyrrolyl<sup>a</sup>**

EA (pyrrolyl) <sup>b</sup>	2.145 ± 0.010 eV
$D_0(\text{pyrrole})^c$	93.92 ± 0.11 kcal mol <sup>-1</sup>
$\Delta_{\text{acid}}H_0(\text{pyrrole})^d$	358.0 ± 0.4 kcal mol <sup>-1</sup>
$\Delta_{\text{acid}}H_{298}(\text{pyrrole})^e$	359.4 ± 0.4 kcal mol <sup>-1</sup>
$\Delta_{\text{acid}}S_{298}(\text{pyrrole})^f$	25.4 cal mol <sup>-1</sup> K <sup>-1</sup>
$\Delta_{\text{acid}}G_{298}(\text{pyrrole})^g$	351.9 ± 0.4 kcal mol <sup>-1</sup>
$\Delta_{\text{acid}}G_{298}(\text{pyrrolyl})^b$	350.9 ± 2.0 kcal mol <sup>-1</sup>

<sup>a</sup> Acidities and bond enthalpies are associated with the N–H hydrogen and N–H bond, respectively. <sup>b</sup> Experimentally determined in the present study. <sup>c</sup> Reference 27. <sup>d</sup> Determined with EA and  $D_0(\text{pyrrole})$  through a thermochemical cycle (see eq 4 in the text). <sup>e</sup> Derived from  $\Delta_{\text{acid}}H_0(\text{pyrrole})$  and thermal correction (see eq 5 in the text). <sup>f</sup> Derived from DFT calculation (B3LYP/6-311++G(d,p)). Unscaled vibrational frequencies were used. <sup>g</sup> Derived from  $\Delta_{\text{acid}}H_{298}(\text{pyrrole})$  and  $\Delta_{\text{acid}}S_{298}(\text{pyrrole})$ .

accurate but in excellent agreement with this value. Table 2 summarizes thermodynamic parameters for pyrrole and pyrrolyl radical.

## Discussion

**Pyrrolyl <sup>2</sup>A<sub>2</sub> Ground State.** The photoelectron spectrum of pyrrolide reflects the optical transition from the initial pyrrolide ground state to the final continuum state composed of pyrrolyl and a photodetached electron. Franck–Condon analysis based on the DFT calculations for the <sup>1</sup>A<sub>1</sub> anion and <sup>2</sup>A<sub>2</sub> radical gives a very good representation of the experimental spectrum (Figure 1a and 1b). The main peaks in the spectrum, besides the origin peak, represent three totally symmetric vibrational modes of the radical, as depicted in Figure 3. These modes are active in the spectrum because a substantial shift in the equilibrium geometry takes place along these normal coordinates in the transition from the anion ground state to the radical ground state.

Pyrrolyl is isoelectronic with cyclopentadienyl. The  $\pi$  orbitals in cyclopentadienyl, analogous to the a<sub>2</sub> and b<sub>1</sub> orbitals illustrated in Figure 2, are degenerate. Replacement of one C–H group with a nitrogen atom converts cyclopentadienyl into pyrrolyl and reduces the maximum symmetry from  $D_{5h}$  to  $C_{2v}$ . Consequently, there is no symmetry requirement that the pyrrolyl  $\pi$  orbitals remain degenerate. As Figure 2 shows, the b<sub>1</sub> orbital of pyrrolyl has a large contribution from the N 2p orbital, while the a<sub>2</sub> orbital essentially consists only of C 2p orbitals. Since the N 2p orbital is more stable than the C 2p orbital, the b<sub>2</sub> orbital will be stabilized compared to the a<sub>2</sub> orbital, leading to a ground state of <sup>2</sup>A<sub>2</sub> for pyrrolyl. Indeed, the <sup>2</sup>A<sub>2</sub> ground state has been found in the ESR measurement for pyrrolyl in aqueous solution.<sup>50</sup> The Franck–Condon analysis of the photoelectron spectrum of pyrrolide confirms this assignment.

It is straightforward to rationalize the geometry change between the anion ground state and the radical ground state by recognizing the nature of the anion orbital from which electron detachment takes place. The a<sub>2</sub> orbital has bonding character between C<sub>2</sub> and C<sub>3</sub> and between C<sub>4</sub> and C<sub>5</sub>, while antibonding character is found between C<sub>3</sub> and C<sub>4</sub> (Figure 2; see the figure for Table 1 for atom numbering). Detachment of an electron from this orbital reduces these bonding and antibonding characters. Thus, the C<sub>2</sub>–C<sub>3</sub> and C<sub>4</sub>–C<sub>5</sub> bonds lengthen, while the C<sub>3</sub>–C<sub>4</sub> bond shortens upon electron photodetachment to form the <sup>2</sup>A<sub>2</sub> ground state of the radical, as found in the DFT calculations (Table 1).

The anisotropy parameter,  $\beta$ , associated with the <sup>2</sup>A<sub>2</sub> peaks in the photoelectron spectrum is about –0.5. The dependence of  $\beta$  on both the character of the orbital from which the electron is detached and on the kinetic energy of the photoelectron is

well-known in atomic systems.<sup>33,51</sup> While the angular and kinetic energy dependence of photoelectrons detached from molecular orbitals is more complicated, one can still learn about the character of the molecular orbitals by comparing the observed  $\beta$  values with that found for well-known molecular systems. Generally, one finds that  $\beta$  is negative for 1–3 eV electrons detached from  $\pi$  molecular orbitals, as observed for the benzyl anion ( $\beta = -0.42$  at an eKE of 2.6 eV) and phenoxide ( $\beta = -0.53$  at an eKE of 1.3 eV).<sup>52</sup> Thus, the anisotropy observed in the major peaks in the pyrrolide photoelectron spectrum is consistent with electron photodetachment from a  $\pi$  (a<sub>2</sub>) orbital to form ground-state pyrrolyl (<sup>2</sup>A<sub>2</sub>).

The photoelectron spectrum of pyrrolide bears a striking resemblance to the photoelectron spectrum of pyrrole, reported in the literature a few decades ago.<sup>53,54</sup> Photoionization of pyrrole results in the formation of pyrrole radical cation (protonated pyrrolyl). The ground state of pyrrole radical cation is <sup>2</sup>A<sub>2</sub>, as with pyrrolyl. We have carried out a Franck–Condon analysis of the pyrrole photoelectron spectrum, using structures and frequencies derived from DFT calculations on pyrrole and pyrrolyl radical cation ground states. This calculated spectrum reproduced the observed spectrum very well, with three active vibrational modes and displacements, all virtually identical to the corresponding modes active in the photoelectron spectrum of pyrrolide. This finding confirms that the geometric change in the transition from the ground state of pyrrole to the ground state of pyrrole radical cation is very similar to that from the pyrrolide ground state to the pyrrolyl ground state. The similarity in the electronic structure of the ground states of pyrrolyl and pyrrole radical cation has also been observed in the ESR spectra.<sup>50,55,56</sup>

**Pyrrolyl <sup>2</sup>B<sub>1</sub> Transition State.** Figure 1b shows that the Franck–Condon simulation of the photoelectron spectrum of <sup>2</sup>B<sub>1</sub> pyrrolyl predicts a prominent, well-resolved photoelectron spectrum<sup>48</sup> beginning about 0.5 eV above the ground-state origin. No such spectrum is observed, but there appears to be a weak continuum in this region. This state is “missing” because of a large imaginary frequency at the <sup>2</sup>B<sub>1</sub> saddle point. The DFT calculation with the <sup>2</sup>B<sub>1</sub> electronic symmetry finds that one b<sub>2</sub> mode has a very large imaginary frequency, 2167i cm<sup>-1</sup>. All other calculated frequencies are real, with the smallest frequency being 326 cm<sup>-1</sup>. The displacements for this imaginary mode are depicted in Figure 3. The magnitude of the imaginary frequency shows the steepness of the potential energy surface along this normal coordinate. It is well known that the shape of the potential energy surface is directly related to lifetime broadening in transition-state spectra.<sup>57</sup> Perhaps it is useful to consider a specific example of such broadening. The <sup>1</sup>A<sub>1g</sub> state of cyclooctatetraene (COT) has a  $D_{4h}$  structure, and it is a transition state for more stable  $D_{2d}$  configurations.<sup>58,59</sup> The imaginary frequency for the COT <sup>1</sup>A<sub>1g</sub> state was calculated to be 90i cm<sup>-1</sup>. The relatively small magnitude of this imaginary frequency indicates that the potential energy surface along this normal coordinate is rather flat, and broadening of the spectrum should be moderate. Indeed, the <sup>1</sup>A<sub>1g</sub> state is manifest in the photoelectron spectrum of COT negative ion with its origin peak and a distinct pair of vibrational peaks well resolved, although there is a slight increase in the width of photoelectron peaks, when compared with the spectrum for the <sup>3</sup>A<sub>2u</sub> state, which is a minimum.

The relatively large magnitude of the imaginary frequency for the pyrrolyl <sup>2</sup>B<sub>1</sub> state suggests that the spectrum would be broadened *substantially*. The Franck–Condon simulation in Figure 1b was performed with an fwhm of 15 meV.<sup>48</sup> This line

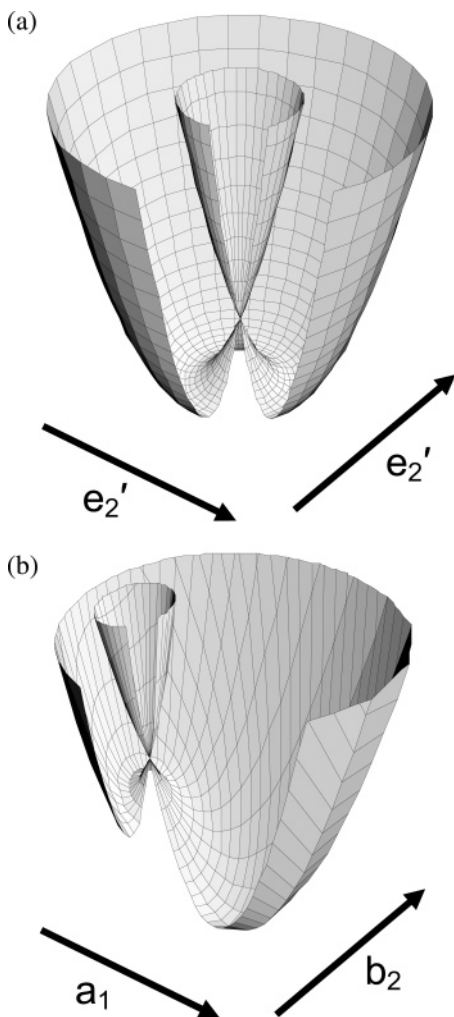


**Figure 4.** Schematic illustration of the potential energy surfaces of the two lowest electronic states of (a) cyclopentadienyl and (b) pyrrolyl.

width represents the instrument resolution and is appropriate for the  ${}^2A_2$  ground state but not for the  ${}^2B_1$  transition state. If the  ${}^2B_1$  state has both substantial lifetime broadening and a cross section comparable to the ground state (as is the case for valence electron ejection), then the spectrum would appear as a weak, broad, featureless continuum, as observed. The Franck–Condon simulation for the  ${}^2A_2$  ground state shows little intensity above 2.7 eV electron binding energy, and yet the experimental spectrum exhibits a weak tail up to about 3.1 eV, with a significantly different anisotropy parameter. Thus, all of these observations lead to the conclusion that the broad tail of the photoelectron spectrum above an electron binding energy of 2.6 eV reflects transitions to the  ${}^2B_1$  transition state, with an intrinsic width of perhaps 0.1 eV.

As mentioned above, there is a similarity between the photoelectron spectra of pyrrolide and pyrrole for the ground states of pyrrolyl and pyrrole radical cation ( ${}^2A_2$ ). The photoelectron spectrum of pyrrole clearly shows a distinctive feature for the  ${}^2B_1$  state of pyrrole radical cation, but the spectrum is quite broad in contrast to the spectrum for the  ${}^2A_2$  state of pyrrole radical cation. The broad  ${}^2B_1$  spectrum for pyrrole radical cation parallels the broad  ${}^2B_1$  spectrum for pyrrolyl. However, the  ${}^2B_1$  state of the pyrrole radical cation is a minimum, not a transition state, as discussed in more detail below.<sup>53</sup>

**The Ground Adiabatic Potential Energy Surface.** The DFT calculations predict a saddle point for the  ${}^2B_1$  electronic symmetry of pyrrolyl with an imaginary frequency for a  $b_2$

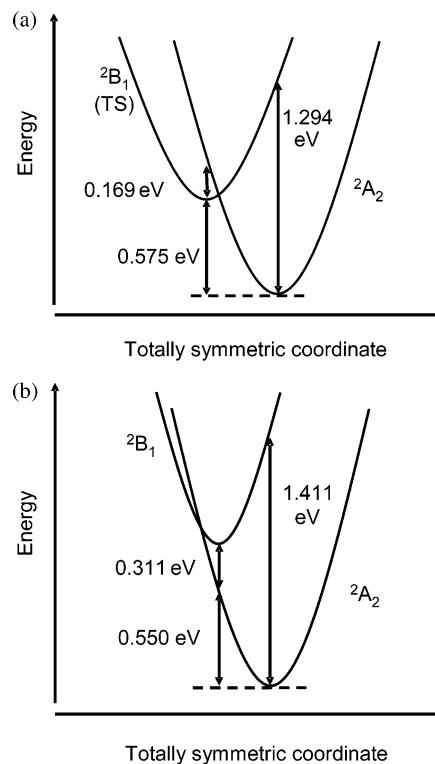


**Figure 5.** Schematic illustration of the potential energy curves of the two lowest electronic states of (a) pyrrolyl radical, corresponding to a slice of the potential energy surfaces shown in Figure 4 along the totally symmetric coordinate, and (b) pyrrole radical cation. The potential energy separations were calculated at B3LYP/6-311++G(d,p) level.

mode. The  ${}^2B_1$  stationary point region of the adiabatic potential energy surface is perturbed by strong vibronic coupling between the  ${}^2A_2$  and  ${}^2B_1$  states.

Again, a comparison between cyclopentadienyl and pyrrolyl is useful. Figure 4a shows a qualitative picture of the adiabatic potential energy surfaces of cyclopentadienyl along first-order Jahn–Teller-active normal coordinates, as discussed most recently by Miller et al.<sup>60,61</sup> The degenerate ground states,  $E_1''$ , in  $D_{5h}$  geometry are subject to Jahn–Teller effects, so the minima are located at  $C_s$  geometries, which form a pseudorotation path on the  $A''$  ground adiabatic potential energy surface (the moat in Figure 4a). It is not apparent in Figure 4a, but this pseudorotation path includes 10  $C_{2v}$  points; five of them have  $A_2$  electronic symmetry and the other five have  $B_1$  electronic symmetry. The conical intersection is located at  $D_{5h}$  geometry. The energy of the conical intersection relative to the minima was determined to be 0.1534 eV through the analysis of vibronic structure in the fluorescence spectrum of cyclopentadienyl.<sup>60,61</sup>

The corresponding adiabatic potential energy surfaces for pyrrolyl can be drawn along  $a_1$  and  $b_2$  normal coordinates, as shown schematically in Figure 4b. The picture reflects the fact that the  $E_1''$  degeneracy has been broken in pyrrolyl, giving rise to a  ${}^2A_2$  minimum and  ${}^2B_1$  saddle point on the  $A''$  ground adiabatic potential energy surface. The imaginary frequency for the  ${}^2B_1$  saddle point is associated with the  $b_2$  normal coordinate. Following the pseudorotation path starting at the  ${}^2B_1$  saddle point, the potential energy surface is downhill all the way to the  ${}^2A_2$  minimum. Figure 4b also portrays the proximity of the  ${}^2B_1$  saddle point and its conical intersection with the  ${}^2A_2$  state.

A one-dimensional slice of the potential energy surfaces of pyrrolyl along the  $C_{2v}$  axis is shown in Figure 5a. B3LYP calculations again were employed to evaluate the energetic relation between the  ${}^2A_2$  and  ${}^2B_1$  electronic symmetries at the

stationary points (Figure 5a). At the  ${}^2A_2$  minimum geometry, the upper potential energy ( ${}^2B_1$ ) is 1.3 eV higher. In contrast, at the  ${}^2B_1$  saddle point geometry, the upper potential energy ( ${}^2A_2$ ) is located only 0.17 eV above the  ${}^2B_1$  saddle point. These differences are important properties to characterize the vibronic coupling and can be used in a standard vibronic coupling model to rationalize the experimental results.

A usual starting point in characterizing adiabatic potential energy surfaces is to expand the Hamiltonian about a reference nuclear configuration in the basis of noncoupled electronic states (i.e., diabatic states); up to second-order,<sup>62</sup> one finds

$$V_i = V_0 + \sum_{\alpha} \left\langle \Psi_i \left| \frac{\partial H}{\partial Q_{\alpha}} \right| \Psi_i \right\rangle Q_{\alpha} + \frac{1}{2} \sum_{\alpha} \left\langle \Psi_i \left| \frac{\partial^2 H}{\partial Q_{\alpha}^2} \right| \Psi_i \right\rangle Q_{\alpha}^2 - \sum_{\alpha, k \neq i} \frac{\left\langle \Psi_i \left| \frac{\partial H}{\partial Q_{\alpha}} \right| \Psi_k \right\rangle \left\langle \Psi_k \left| \frac{\partial H}{\partial Q_{\alpha}} \right| \Psi_i \right\rangle}{E_k - E_i} Q_{\alpha}^2 \quad (6)$$

Here, the index  $\alpha$  covers all the normal modes while  $k$  describes all the relevant electronic states. The last term in eq 6 is the vibronic coupling term. In the pyrrolyl system, the two relevant electronic states are  ${}^2A_2$  and  ${}^2B_1$ . Then, the matrix elements in the vibronic coupling term are nonzero only when the nuclear coordinate is a  $b_2$  mode. When the  ${}^2B_1$  saddle point geometry is taken as the reference, the energy separation of  ${}^2A_2$  and  ${}^2B_1$  (the denominator of the vibronic term) is quite small, and the vibronic coupling term is rather large in magnitude. For the ground adiabatic potential energy surface, the vibronic term is negative, and if the magnitude of the vibronic term exceeds that of the other quadratic term, the reference configuration turns into a saddle point. The imaginary frequency of  $2167i$   $\text{cm}^{-1}$  for a  $b_2$  mode for the  ${}^2B_1$  electronic symmetry is consistent with this idea (but see below). On the other hand, the relatively large energy separation at the  ${}^2A_2$  minimum geometry suggests that there will be only minor vibronic coupling effects on the adiabatic potential energy surface near the minimum geometry. This region is, of course, the portion of configuration space explored in the photoelectron spectrum of the  ${}^2A_2$  ground state.

For comparison, Figure 5b illustrates the corresponding potential energy curves for pyrrole radical cation. The  ${}^2B_1$  potential energy is 0.31 eV higher than the  ${}^2A_2$  potential energy at the  ${}^2B_1$  minimum geometry of pyrrole radical cation.<sup>63</sup> Notice that the energy ordering is opposite from that for pyrrolyl at the  ${}^2B_1$  saddle point geometry; the  ${}^2B_1$  minimum is located on the upper adiabatic potential energy surface. The sign of the vibronic coupling term in eq 6 is positive for the upper adiabatic potential energy surface. Thus, vibronic coupling makes the upper potential energy surface steeper. Indeed, B3LYP/6-311++G(d,p) calculations on pyrrole radical cation found that the  ${}^2B_1$  state is a minimum, but one  $b_2$  mode has an unusually large frequency of  $4703$   $\text{cm}^{-1}$  (but see below). Following the classification of Muller, Koppel, and Cederbaum, pyrrole radical cation has “weakly shifted potential energy surfaces”, and pyrrolyl has “strongly shifted potential energy surfaces”.<sup>64</sup> It should be remembered that the photoelectron spectrum for the  ${}^2B_1$  pyrrole radical cation has quite a broad line width even though it is not a transition state.<sup>53</sup> Strong vibronic coupling between the vibrational levels of the  ${}^2B_1$  state and the dense vibrational levels of the  ${}^2A_2$  state around the  ${}^2B_1$  minimum

geometry can spread the transition intensity among a large number of vibronic levels, making the  ${}^2B_1$  spectrum appear broad.<sup>65</sup>

In the above discussion, the results of DFT harmonic vibrational frequency calculations are employed to argue for the pseudo-Jahn–Teller effects in pyrrolyl as well as pyrrole radical cation. The arguments, however, are qualitative in nature. The most obvious sign of the qualitative nature comes from the unphysical IR intensity of the  $b_2$  mode with a frequency of  $4703$   $\text{cm}^{-1}$  for the  ${}^2B_1$  state of pyrrole radical cation. The results of the harmonic vibrational frequency analysis are provided in Supporting Information. In Hartree–Fock methods (and post-Hartree–Fock methods), artifactual symmetry breaking is ubiquitous,<sup>66–68</sup> particularly in open-shell systems. The orbital instability can interfere with correct prediction of the pole structure of the force constant.<sup>66–72</sup> The situation may be similar in DFT calculations.<sup>73–77</sup> Recently, Crawford studied this problem in BNB and  $C_3^+$  molecules using DFT calculations.<sup>78</sup>

Strong pseudo-Jahn–Teller effects in pyrrolyl and pyrrole radical cation can be verified by CASSCF frequency analysis, as proposed by Robb and co-workers.<sup>79</sup> To this end, CASSCF-(7,6) calculations were carried out using Gaussian 98,<sup>41</sup> including five valence  $\pi$  orbitals and one  $\sigma$  orbital in the active space. When no electronic symmetry restriction is imposed on configuration state functions (CSF), a transition state is found with  $B_1$  electronic symmetry with a  $b_2$  imaginary frequency of  $1769i$   $\text{cm}^{-1}$  for pyrrolyl. However, when CSF of  $A_2$  electronic symmetry are removed, a minimum is found with  $B_1$  electronic symmetry, with the smallest  $b_2$  frequency of  $934$   $\text{cm}^{-1}$ . Exclusion of  $A_2$  CSF removes pseudo-Jahn–Teller interactions between the  $A_2$  and  $B_1$  electronic symmetries from the Hessian calculation. Similarly, for the  ${}^2B_1$  state of pyrrole radical cation, one  $b_2$  mode with a frequency of  $1753$   $\text{cm}^{-1}$  in the absence of  $A_2$  electronic symmetry in CSF demonstrates significant increase in the frequency (by more than  $1000$   $\text{cm}^{-1}$ ) when no electronic symmetry restriction is imposed on CSF. These CASSCF results are available in Supporting Information. Thus, CASSCF analysis corroborates the idea that the pseudo-Jahn–Teller effects are substantial in both pyrrolyl and pyrrole radical cation.

An attempt was made to learn how close the conical intersection lies to the  ${}^2B_1$  saddle point in pyrrolyl. Algorithms to locate conical intersection points have been developed and reported in the literature.<sup>80–82</sup> First, the state-averaged (SA) CASSCF method,<sup>81</sup> available in the Gaussian 98 suite of programs,<sup>41</sup> was employed here. The conical intersection was  $0.122$  eV above the  ${}^2B_1$  stationary point with SA-CASSCF/6-311++G(d,p). However, there is a serious concern about this method, because it does not account for dynamic electron correlation. Indeed, significant differences were found in the B3LYP and CASSCF optimized geometries for the  ${}^2A_2$  and  ${}^2B_1$  states. The conical intersection, calculated at B3LYP//SA-CASSCF, was lower in energy than the  ${}^2B_1$  saddle point, calculated at B3LYP//B3LYP. Thus, the SA-CASSCF method is not meaningful in this context. The energy of the conical intersection calculated with SA-CASSCF for cyclopentadienyl is much larger than that determined from experiments.<sup>60,61,83</sup> Perhaps, calculations with the multireference configuration interaction method as described by Yarkony would be more reliable, but this is beyond the scope of the present study.

As an alternative, the method developed by Koppel et al.,<sup>65</sup> in which the geometry and energy of the conical intersection were evaluated according to analytical expressions, was employed. Model potentials were used for the two relevant states, expanded with respect to the normal coordinates of a reference



state, pyrrolide anion ground state. The potentials were assumed to be harmonic and linear coupling was assumed in the model. All parameters required in the analytical expressions were calculated at the B3LYP/6-311++G(d,p) level of theory. The conical intersection was evaluated to be 0.005 eV above the energy of the  ${}^2B_1$  transition state. However, a strange geometry was found for the conical intersection. All bond lengths were very close to those of the  ${}^2B_1$  state, which is reasonable considering the energetic proximity of the conical intersection to the  ${}^2B_1$  saddle point, but the bond angles were closer to those found for the  ${}^2A_2$  state. This result was puzzling and we suspect that the linear coupling approximation may not be adequate when the conical intersection is located very close to one of the stationary points while the reference state is rather distant.

Finally, a primitive, but intuitively pleasing, approach to estimate the energy of the conical intersection was explored. The atomic displacements between the geometries of the  ${}^2A_2$  and  ${}^2B_1$  stationary points were calculated, and this set of relative displacements was taken to represent a totally symmetric mode. The geometry was displaced along this coordinate to find the curve crossing between the two states at the B3LYP level of theory. This curve crossing can be regarded as the  $C_{2v}$  conical intersection minimum. The resultant geometry parameters are given in Table 1. According to this procedure, the conical intersection is located 0.010 eV above the  ${}^2B_1$  saddle point. This number for pyrrolyl should be a reasonable approximation to the true conical intersection minimum because the conical intersection is often close to the line linearly connecting the two stationary points in the multidimensional space.<sup>84</sup> From this full set of calculations, we conclude that the energy of the conical intersection is very close ( $\sim 0.010$  eV) to that of the  ${}^2B_1$  saddle point.

To give perspective on the conical intersection of pyrrolyl, consider the known conical intersection of  $NO_2$ . The  ${}^2A_1$  ground state and the  ${}^2B_2$  excited state of  $NO_2$  interact through vibronic coupling, and this interaction has been the subject of numerous experimental and theoretical studies.<sup>84–98</sup> Mahapatra et al. carried out ab initio calculations to elucidate the effect of vibronic coupling on the photoelectron spectrum of  $NO_2^-$ .<sup>98</sup> They used a model potential technique described above, and the conical intersection was estimated to be 0.049 eV higher in energy than the  ${}^2B_2$  stationary point. The  ${}^2B_2$  state of  $NO_2$  is a minimum, not a transition state. A much smaller energy separation ( $\sim 0.010$  eV) between the conical intersection and the  ${}^2B_1$  saddle point found in pyrrolyl is consistent with the idea that the vibronic coupling effect is much more prominent in pyrrolyl, so much so that it transforms the  ${}^2B_1$  state into a transition state.

**Thermodynamics.** In our laboratories, we have carried out gas-phase acidity and EA measurements to determine the R–H bond dissociation energy (BDE) for several chemical systems<sup>99–101</sup> through a thermochemical cycle (eq 4).<sup>25,26</sup> Usually, the largest uncertainty in the determination of the BDE arises from the gas-phase acidity measurements when the reference acid has a large uncertainty in the acidity value. There have been a few conflicting reports on the N–H BDE of pyrrole.<sup>40,102,103</sup> Ashfold recently determined the N–H BDE for pyrrole with an uncertainty of less than 0.010 eV.<sup>27</sup> When combined with the present EA of pyrrolyl, the gas-phase acidity of pyrrole is determined quite accurately,  $\Delta_{\text{acid}}G_{298}(\text{pyrrole}) = 351.9 \pm 0.4$  kcal mol<sup>-1</sup>. The gas-phase acidity determined in the present ion kinetics measurements is in excellent agreement with this value (Table 2).

Conversely, the equilibrium measurements now allow for a more accurate determination of  $\Delta_{\text{acid}}G_{298}(\text{CH}_3\text{SH})$  by using  $\Delta_{\text{acid}}G_{298}(\text{pyrrole})$  determined through the thermochemical cycle as the reference. These results yield  $\Delta_{\text{acid}}G_{298}(\text{CH}_3\text{SH}) = 351.6 \pm 0.4$  kcal mol<sup>-1</sup>. Methanethiol is one of the anchor molecules in the gas-phase relative acidity scale,<sup>22</sup> of which the reported absolute acidity is  $\Delta_{\text{acid}}G_{298} = 350.6 \pm 2.0$  kcal mol<sup>-1</sup>.<sup>36</sup> This value was determined using eq 4 and an entropy calculation, and the large uncertainty ( $\pm 2.0$  kcal mol<sup>-1</sup>) arises almost exclusively from that in the S–H BDE value for  $\text{CH}_3\text{SH}$ .<sup>22</sup> This current study has measured the acidity difference between pyrrole and  $\text{CH}_3\text{SH}$  as 0.3 kcal mol<sup>-1</sup>, in perfect agreement with the original measurement.<sup>22</sup> Therefore, the new N–H BDE of Ashfold combined with the present EA measurement revises the absolute gas-phase acidity for  $\text{CH}_3\text{SH}$  by 1.0 kcal mol<sup>-1</sup> with substantially improved accuracy. This will alter the acidity values for other molecules that have been referenced by methanethiol (e.g.,  $\text{CH}_3\text{NO}_2$  and  $\text{C}_2\text{H}_5\text{NO}_2$ ) along with the acidity of another anchor molecule  $\text{C}_2\text{H}_5\text{SH}$ , for which the relative acidity has also been measured in reference to  $\text{CH}_3\text{SH}$ .<sup>22</sup>

## Conclusion

The photoelectron spectrum of pyrrolide has been measured, and the EA of pyrrolyl has been determined to be  $2.145 \pm 0.010$  eV. This EA value and the N–H BDE of pyrrole reported by Ashfold<sup>27</sup> were combined in a thermochemical cycle to determine the gas-phase acidity of pyrrole:  $\Delta_{\text{acid}}G_{298}(\text{RH}) = 351.9 \pm 0.4$  kcal mol<sup>-1</sup> and  $\Delta_{\text{acid}}H_{298}(\text{RH}) = 359.4 \pm 0.4$  kcal mol<sup>-1</sup>. The rate constants have been measured for the proton-transfer reactions in the system of pyrrole and methanethiol, and the gas-phase acidity of pyrrole has been determined using that of methanethiol as a reference. The gas-phase acidity of pyrrole so obtained is in excellent agreement with that determined through the thermochemical cycle. These results may be combined, instead, to provide a more accurate measure of the gas-phase acidity of methanethiol,  $\Delta_{\text{acid}}G_{298}(\text{CH}_3\text{SH}) = 351.6 \pm 0.4$  kcal mol<sup>-1</sup>.

The photoelectron spectrum of pyrrolide provides useful information about both the structure and potential energy surface of pyrrolyl. The Franck–Condon simulation of the spectrum based on B3LYP/6-311++G(d,p) calculations for pyrrolide and pyrrolyl confirms that the ground state of pyrrolyl is  ${}^2A_2$  and identifies three harmonic vibrational frequencies active in the spectrum ( $925 \pm 65$ ,  $1012 \pm 25$ , and  $1464 \pm 20$  cm<sup>-1</sup>). These totally symmetric modes of  ${}^2A_2$  pyrrolyl have large displacements along the ring coordinates.

On the other hand, the first excited state of pyrrolyl,  ${}^2B_1$ , appears broad and featureless, overlapping the tail of the  ${}^2A_2$  portion of the spectrum. The DFT calculations predict a saddle point for the  ${}^2B_1$  electronic symmetry, reflecting strong vibronic coupling with the  ${}^2A_2$  state. The imaginary frequency for a  $b_2$  mode is calculated to be  $2167i$  cm<sup>-1</sup>, indicating that the ground adiabatic potential energy surface is rather steep along this normal coordinate. Consequently, lifetime broadening is quite substantial, which can explain the observed spectrum for the  ${}^2B_1$  transition state. The term energy for the  ${}^2B_1$  state is 0.49 eV according to the DFT calculations, but this energy cannot be determined from the observed spectrum. Comparison has been made between pyrrolyl and an isoelectronic species, cyclopentadienyl, with respect to the two lowest electronic states. This comparison illustrates the effect N atom substitution has on the molecular orbitals as well as on the potential energy surface. In addition, the difference in the role of vibronic



coupling has been discussed between pyrrolyl and pyrrole radical cation (i.e., protonated pyrrolyl radical).

The present study represents our initial step in an attempt to understand how chemical properties change as N atoms replace CH groups in the five-membered aromatic species. Currently, we are undertaking studies on the systems with two nitrogen atoms in the five-membered ring (i.e., pyrazole and imidazole), which will be published in forthcoming papers.

**Acknowledgment.** We are grateful to Professor Michael Ashfold for sharing his unpublished data on the N–H BDE of pyrrole. We are pleased to acknowledge Professor John Stanton for discussions on the issue of vibronic coupling. We are also indebted to Professor Barney Ellison for useful discussions. This manuscript benefited from useful comments made by two referees. This work was supported by the Air Force Office of Scientific Research and by the National Science Foundation (CHE-0349937).

**Supporting Information Available:** The results of harmonic vibrational analysis for the  ${}^2B_1$  states of pyrrolyl and pyrrole radical cation are provided. The calculations were performed with B3LYP/6-311++G(d,p) and CASSCF(7,6)/6-311++G(d,p). The CASSCF calculations were performed under different electronic symmetry conditions on configuration state functions. This material is available free of charge via the Internet at <http://pubs.acs.org>.

## References and Notes

- Saxe, P.; Schaefer, H. F. *J. Am. Chem. Soc.* **1983**, *105*, 1760.
- Wang, L. J.; Warburton, P.; Mezey, P. G. *J. Phys. Chem. A* **2002**, *106*, 2748.
- Lauderdale, W. J.; Stanton, J. F.; Bartlett, R. J. *J. Phys. Chem.* **1992**, *96*, 1173.
- Fau, S.; Wilson, K. J.; Bartlett, R. J. *J. Phys. Chem. A* **2002**, *106*, 4639.
- Gagliardi, L.; Orlandi, G.; Evangelisti, S.; Roos, B. O. *J. Chem. Phys.* **2001**, *114*, 10733.
- Benin, V.; Kaszynski, P.; Radziszewski, J. G. *J. Org. Chem.* **2002**, *67*, 1354.
- Nguyen, M. T.; Ha, T. K. *Chem. Phys. Lett.* **2001**, *335*, 311.
- Bartlett, R. J. *Chem. Ind.* **2000**, 140.
- Klapotke, T. M. *Angew. Chem., Int. Ed.* **1999**, *38*, 2536.
- Glukhovtsev, M. N.; Jiao, H. J.; Schleyer, P. V. *Inorg. Chem.* **1996**, *35*, 7124.
- Nguyen, M. T.; Ha, T. K. *Chem. Ber.* **1996**, *129*, 1157.
- Zheng, J. P.; Waluk, J.; Spanget-Larsen, J.; Blake, D. M.; Radziszewski, J. G. *Chem. Phys. Lett.* **2000**, *328*, 227.
- Cacace, F.; de Petris, G.; Troiani, A. *Science* **2002**, *295*, 480.
- Christe, K. O.; Wilson, W. W.; Sheehy, J. A.; Boatz, J. A. *Angew. Chem., Int. Ed.* **1999**, *38*, 2004.
- Vij, A.; Wilson, W. W.; Vij, V.; Tham, F. S.; Sheehy, J. A.; Christe, K. O. *J. Am. Chem. Soc.* **2001**, *123*, 6308.
- Vij, A.; Pavlovich, J. G.; Wilson, W. W.; Vij, V.; Christe, K. O. *Angew. Chem., Int. Ed.* **2002**, *41*, 3051.
- Ostmark, H.; Wallin, S.; Brinck, T.; Carlqvist, P.; Claridge, R.; Hedlund, E.; Yudina, L. *Chem. Phys. Lett.* **2003**, *379*, 539.
- Alfassi, Z. B.; Schuler, R. H. *J. Phys. Chem.* **1985**, *89*, 3359.
- Workentin, M. S.; Wagner, B. D.; Negri, F.; Zgierski, M. Z.; Luszyk, J.; Siebrand, W.; Wayner, D. D. M. *J. Phys. Chem.* **1995**, *99*, 94.
- Workentin, M. S.; Wagner, B. D.; Luszyk, J.; Wayner, D. D. M. *J. Am. Chem. Soc.* **1995**, *117*, 119.
- Butler, R. N.; Stephens, J. C.; Burke, L. A. *Chem. Commun.* **2003**, 1016.
- Bartmess, J. E.; Scott, J. A.; McIver, R. T. *J. Am. Chem. Soc.* **1979**, *101*, 6046.
- Engelking, P. C.; Lineberger, W. C. *J. Chem. Phys.* **1977**, *67*, 1412.
- McMillen, D. F.; Golden, D. M. *Annu. Rev. Phys. Chem.* **1982**, *33*, 493.
- Berkowitz, J.; Ellison, G. B.; Gutman, D. *J. Phys. Chem.* **1994**, *98*, 2744.
- Blanksby, S. J.; Ellison, G. B. *Acc. Chem. Res.* **2003**, *36*, 255.
- Ashfold, M. N. R. Private communication, to be published; for a preliminary account see Blancfort, Temps, et al. *Faraday Discuss.* **2004**, *127*, 355.
- Ervin, K. M.; Lineberger, W. C. Photoelectron Spectroscopy of Negative Ions. In *Advances in Gas Phase Ion Chemistry*; Adams, N. G., Babcock, L. M., Eds.; JAI Press: Greenwich, 1992; Vol. 1, p 121.
- Leopold, D. G.; Murray, K. K.; Stevens-Miller, A. E.; Lineberger, W. C. *J. Chem. Phys.* **1985**, *83*, 4849.
- Ervin, K. M.; Ho, J.; Lineberger, W. C. *J. Chem. Phys.* **1989**, *91*, 5974.
- Neumark, D. M.; Lykke, K. R.; Andersen, T.; Lineberger, W. C. *Phys. Rev. A* **1985**, *32*, 1890.
- Moore, C. E. *Atomic Energy Levels*; US GPO Circular No. 467: Washington, 1952.
- Cooper, J.; Zare, R. N. *J. Chem. Phys.* **1968**, *48*, 942.
- Van Doren, J. M.; Barlow, S. E.; DePuy, C. H.; Bierbaum, V. M. *Int. J. Mass Spectrom. Ion Processes* **1987**, *81*, 85.
- Bierbaum, V. M. *Encyc. Mass Spectrom.* **2003**, *1*, 98.
- NIST Standard Reference Database Number 69, March 2003 Release.
- Su, T.; Chesnavich, W. J. *J. Chem. Phys.* **1982**, *76*, 5183.
- Miller, K. J.; Savchik, J. A. *J. Am. Chem. Soc.* **1979**, *101*, 7206.
- CRC Handbook of Chemistry and Physics*, 75th ed.; CRC Press: Boca Raton, FL, 1994.
- Richardson, J. H.; Stephenson, L. M.; Brauman, J. I. *J. Am. Chem. Soc.* **1975**, *97*, 1160.
- Frisch, M. J.; Trucks, G. W.; Schlegel, H. B.; Scuseria, G. E.; Robb, M. A.; Cheeseman, J. R.; Zakrzewski, V. G.; Montgomery, J. A.; Stratmann, R. E.; Burant, J. C.; Dapprich, S.; Millam, J. M.; Daniels, A. D.; Kudin, K. N.; Strain, M. C.; Farkas, O.; Tomasi, J.; Barone, V.; Cossi, M.; Cammi, R.; Mennucci, B.; Pomelli, C.; Adamo, C.; Clifford, S.; Ochterski, J.; Peterson, G. A.; Ayala, P. Y.; Cui, Q.; Morokuma, K.; Malick, D. K.; Rabuck, A. D.; Raghavachari, K.; Foresman, J. B.; Cioslowski, J.; Ortiz, J. V.; Baboul, A. G.; Stefanov, B. B.; Liu, G.; Liashenko, A.; Piskorz, P.; Komaromi, I.; Gomperts, R.; Martin, R. L.; Fox, D. J.; Keith, T.; Al-Laham, M. A.; Peng, C. Y.; Nanayakkara, A.; Gonzalez, C.; Challacombe, M.; Gill, P. M. W.; Johnson, B.; Chen, W.; Wong, M. W.; Andres, J. L.; Gonzalez, C.; Head-Gordon, M.; Replogle, E. S.; Pople, J. *Gaussian 98*, Revision A.9; Gaussian, Inc.: Pittsburgh, PA, 1998.
- Becke, A. D. *J. Chem. Phys.* **1993**, *98*, 5648.
- Lee, C. T.; Yang, W. T.; Parr, R. G. *Phys. Rev. B* **1988**, *37*, 785.
- Krishnan, R.; Binkley, J. S.; Seeger, R.; Pople, J. A. *J. Chem. Phys.* **1980**, *72*, 650.
- Rienstra-Kiracofe, J. C.; Graham, D. E.; Schaefer, H. F. *Mol. Phys.* **1998**, *94*, 767.
- Ervin, K. M. *PESCAL, Fortran program*, 2003.
- Ervin, K. M.; Ramond, T. M.; Davico, G. E.; Schwartz, R. L.; Casey, S. M.; Lineberger, W. C. *J. Phys. Chem. A* **2001**, *105*, 10822.
- The Franck–Condon analysis of the  ${}^2B_1$  spectrum did not include the  $b_2$  mode that has an imaginary frequency.
- The  ${}^2B_1$  term energy for pyrrolyl has been calculated to be between 0.5 and 0.6 eV depending on the level of the theory. See Bacskay, G. B.; Martoprawiro, M.; Mackie, J. C. *Chem. Phys. Lett.* **1998**, *290*, 391.
- Samuni, A.; Neta, P. *J. Phys. Chem.* **1973**, *77*, 1629.
- Hall, J. L.; Siegel, M. W. *J. Chem. Phys.* **1968**, *48*, 943.
- Gunion, R. F.; Gilles, M. K.; Polak, M. L.; Lineberger, W. C. *Int. J. Mass Spectrom. Ion Processes* **1992**, *117*, 601.
- Derrick, P. J.; Asbrink, L.; Edqvist, O.; Lindholm, E. *Spectrochim. Acta, Part A* **1971**, *A 27*, 2525.
- Palmer, M. H.; Walker, I. C.; Guest, M. F. *Chem. Phys.* **1998**, *238*, 179.
- Rao, D. N. R.; Symons, M. C. R. *J. Chem. Soc., Perkin Trans. 2* **1983**, *2*, 135.
- Shiotani, M.; Nagata, Y.; Tadaki, M.; Sohma, J.; Shida, T. *J. Phys. Chem.* **1983**, *87*, 1170.
- Neumark, D. M. *Acc. Chem. Res.* **1993**, *26*, 33.
- Wenthold, P. G.; Hrovat, D. A.; Borden, W. T.; Lineberger, W. C. *Science* **1996**, *272*, 1456.
- Wenthold, P. G.; Lineberger, W. C. *Acc. Chem. Res.* **1999**, *32*, 597.
- Applegate, B. E.; Miller, T. A.; Barckholtz, T. A. *J. Chem. Phys.* **2001**, *114*, 4855.
- Applegate, B. E.; Bezant, A. J.; Miller, T. A. *J. Chem. Phys.* **2001**, *114*, 4869.
- Pearson, R. G. *J. Am. Chem. Soc.* **1969**, *91*, 4947.
- The DFT calculations predict that the  ${}^2B_1$  term energy is 1.08 eV (with zero point energy corrections) for pyrrole radical cation, in excellent agreement with the experimental value (see ref 53).
- Muller, H.; Koppel, H.; Cederbaum, L. S. *New J. Chem.* **1993**, *17*, 7.
- Koppel, H.; Domcke, W.; Cederbaum, L. S. *Adv. Chem. Phys.* **1984**, *57*, 59.
- Allen, W. D.; Horner, D. A.; Dekock, R. L.; Remington, R. B.; Schaefer, H. F. *Chem. Phys.* **1989**, *133*, 11.
- Yamaguchi, Y.; Alberts, I. L.; Goddard, J. D.; Schaefer, H. F. *Chem. Phys.* **1990**, *147*, 309.

- (68) Crawford, T. D.; Stanton, J. F.; Allen, W. D.; Schaefer, H. F. *J. Chem. Phys.* **1997**, *107*, 10626.
- (69) Burton, N. A.; Yamaguchi, Y.; Alberts, I. L.; Schaefer, H. F. *J. Chem. Phys.* **1991**, *95*, 7466.
- (70) Crawford, T. D.; Stanton, J. F.; Szalay, P. G.; Schaefer, H. F. *J. Chem. Phys.* **1997**, *107*, 2525.
- (71) Crawford, T. D.; Stanton, J. F. *J. Chem. Phys.* **2000**, *112*, 7873.
- (72) Stanton, J. F. *J. Chem. Phys.* **2001**, *115*, 10382.
- (73) Bauernschmitt, R.; Ahlrichs, R. *J. Chem. Phys.* **1996**, *104*, 9047.
- (74) Sherrill, C. D.; Lee, M. S.; Head-Gordon, M. *Chem. Phys. Lett.* **1999**, *302*, 425.
- (75) Cohen, R. D.; Sherrill, C. D. *J. Chem. Phys.* **2001**, *114*, 8257.
- (76) Byrd, E. F. C.; Sherrill, C. D.; Head-Gordon, M. *J. Phys. Chem. A* **2001**, *105*, 9736.
- (77) Orlova, G.; Goddard, J. D. *Chem. Phys. Lett.* **2002**, *363*, 486.
- (78) Russ, N. J.; Crawford, T. D.; Tschumper, G. S. *J. Chem. Phys.* **2004**, *120*, 7298.
- (79) Bearpark, M. J.; Blancafort, L.; Robb, M. A. *Mol. Phys.* **2002**, *100*, 1735.
- (80) Lengsfeld, B. H.; Yarkony, D. R. *Adv. Chem. Phys.* **1992**, *82*, 1.
- (81) Bearpark, M. J.; Robb, M. A.; Schlegel, H. B. *Chem. Phys. Lett.* **1994**, *223*, 269.
- (82) Yarkony, D. R. Electronic Structure Aspects of Nonadiabatic Processes in Polyatomic Systems. In *Modern Electronic Structure Theory, Part I*; Yarkony, D. R., Ed.; World Scientific: Singapore, 1995; p 642.
- (83) Bearpark, M. J.; Robb, M. A.; Yamamoto, N. *Spectrochim. Acta, Part A* **1999**, *55*, 639.
- (84) Mahapatra, S.; Koppel, H.; Cederbaum, L. S.; Stampfuss, P.; Wenzel, W. *Chem. Phys.* **2000**, *259*, 211.
- (85) Smalley, R. E.; Wharton, L.; Levy, D. H. *J. Chem. Phys.* **1975**, *63*, 4977.
- (86) Jackels, C. F.; Davidson, E. R. *J. Chem. Phys.* **1976**, *64*, 2909.
- (87) Jackels, C. F.; Davidson, E. R. *J. Chem. Phys.* **1976**, *65*, 2941.
- (88) Ervin, K. M.; Ho, J.; Lineberger, W. C. *J. Phys. Chem.* **1988**, *92*, 5405.
- (89) Weaver, A.; Metz, R. B.; Bradforth, S. E.; Neumark, D. M. *J. Chem. Phys.* **1989**, *90*, 2070.
- (90) Kaldor, U. *Chem. Phys. Lett.* **1990**, *170*, 17.
- (91) Kaldor, U. *Chem. Phys. Lett.* **1991**, *185*, 131.
- (92) Delon, A.; Jost, R. *J. Chem. Phys.* **1991**, *95*, 5686.
- (93) Georges, R.; Delon, A.; Bylicki, F.; Jost, R.; Campargue, A.; Charvat, A.; Chenevier, M.; Stoeckel, F. *Chem. Phys.* **1995**, *190*, 207.
- (94) Georges, R.; Delon, A.; Jost, R. *J. Chem. Phys.* **1995**, *103*, 1732.
- (95) Delon, A.; Georges, R.; Jost, R. *J. Chem. Phys.* **1995**, *103*, 7740.
- (96) Leonardi, E.; Petrongolo, C.; Hirsch, G.; Buenker, R. J. *J. Chem. Phys.* **1996**, *105*, 9051.
- (97) Leonardi, E.; Petrongolo, C. *J. Chem. Phys.* **1997**, *106*, 10066.
- (98) Mahapatra, S.; Koppel, H.; Cederbaum, L. S. *J. Chem. Phys.* **1999**, *110*, 5691.
- (99) Robinson, M. S.; Polak, M. L.; Bierbaum, V. M.; DePuy, C. H.; Lineberger, W. C. *J. Am. Chem. Soc.* **1995**, *117*, 6766.
- (100) Lee, H. S.; DePuy, C. H.; Bierbaum, V. M. *J. Am. Chem. Soc.* **1996**, *118*, 5068.
- (101) Gunion, R. F.; Karney, W.; Wenthold, P. G.; Borden, W. T.; Lineberger, W. C. *J. Am. Chem. Soc.* **1996**, *118*, 5074.
- (102) Blank, D. A.; North, S. W.; Lee, Y. T. *Chem. Phys.* **1994**, *187*, 35.
- (103) Wei, J.; Kuczmann, A.; Riedel, J.; Renth, F.; Temps, F. *Phys. Chem. Chem. Phys.* **2003**, *5*, 315.